PERGAMON

International Journal of Heat and Mass Transfer 43 (2000) 3513–3527

International Journal of HEAT and MASS TRANSFER

www.elsevier.com/locate/ijhmt

Analysis of momentum and energy transfer in a lid-driven cavity filled with a porous medium

Abdalla M. Al-Amiri*, [1]

Mechanical Engineering Department, The United Arab Emirates University, P.O. Box 17555, Al-Ain, United Arab Emirates

Received 23 June 1999; received in revised form 13 December 1999

Abstract

The laminar transport processes in a lid-driven square cavity filled with a water-saturated porous medium is presented in this numerical investigation. A stable thermal stratification configuration is considered by imposing a vertical temperature gradient. The general formulation of the momentum equation is used such that both the inertial and viscous effects are incorporated. The relevant momentum and energy characteristics of the porous system are identified with special consideration being given to the implications of the inertial effects. The Grashof number in this study was fixed at 10^4. A Nusselt number correlation is established based on the numerical results in the parametric domain of $Da = 0.001 - 0.1$ and $Ri = 10^{-4} - 5.0$.

Keywords: Lid-driven flows; Porous media

1. Introduction

The problem of lid-driven flows in cavities has been a major topic for research studies due to its fundamental nature and owing to the wide spectrum of engineering applications that are associated with it. Examples of such applications can be traced to oil extraction, thermal management of electronic cooling and improvement of performance of heat exchangers. The simple rectangular geometry is often considered for analyzing the momentum and energy transport processes inside the cavity. The flow is induced by sliding the top horizontal wall at a constant speed, while the heat transfer is triggered by sustaining a temperature gradient between the top and bottom walls.

Many numerical techniques have been proposed to tackle this fundamental problem [1–5]. Meanwhile, Koseff and Street [6] and Prasad and Koseff [7] have performed experimental investigations of mixed convection laminar flows past two-dimensional rectangular cavities. Most of the existing studies in the literature on mixed convection lid-driven flows have been dedicated to situations where the fluid flow is not hampered by any porous structure being placed inside the cavity. An exception to this is the numerical study reported by Vafai and Huang [8], which analyzes the effect of forced convection over intermittently emplaced porous cavities. The utilization of a porous substrate for heat transfer augmentation is an attractive choice given that the effective thermal conductivity of the porous structure could be several order of magnitudes higher than the working fluid. Vafai and Huang [8]

* Tel.: +9713-705-1562; fax: +9713-623-158.

E-mail address: alamiri@uaeu.ac.ae (A.M. Al-Amiri).

[1] Please note that his previous publications appeared under the last name of "Amiri".

0017-9310/00/$ - see front matter
PII: S0017-9310(99)00391-9

Nomenclature

B	coefficient of stagnant conductivity
c	specific heat at constant pressure (J kg^{-1} K^{-1})
d_p	sphere particle diameter (m)
Da	Darcy number, K/H^2
F	geometric function defined in Eq. (4)
$\vec{g}$	gravitational acceleration vector (m s^{-2})
Gr	Grashof number, $g\beta\Delta TH^3/\nu_f^2$
H	side length of the cavity (m)
k	thermal conductivity (W m^{-1} K^{-1})
K	permeability (m^2)
Nu	Nusselt number
Pr	Prandtl number, ν_f/α_f
Pe	Peclet number, $U_o H/\nu_f$
Re	Reynolds number, $U_o H/\nu_f$
Ri	Richardson number, Gr/Re^2
t	time (s)
T	temperature (K)
u,v	interstitial velocity components (m s^{-1})
$\mathbf{v}$	interstitial velocity vector (m s^{-1})
V, U	dimensionless interstitial velocity components
x, y	Cartesian coordinates (m)
X, Y	dimensionless coordinates

Greek symbols

α	thermal diffusivity (m^2 s^{-1})
β	thermal expansion coefficient (K^{-1})
ε	porosity
λ	solid-to-fluid thermal conductivity ratio
μ_f	dynamic viscosity (Ns m^{-2})
ν_f	kinematic viscosity (m^2 s^{-1})
θ	dimensionless temperature, $(T-T_c)/(T_h-T_c)$
Ω	vorticity (s^{-1})
ω	dimensionless vorticity, $\Omega H/U_0$
ψ	stream function (m^2 s^{-1})
Ψ	dimensionless stream function, ψ/HU_0
ρ	density (kg m^{-3})
σ	capacity ratio, $[\varepsilon(\rho c)_f+(1-\varepsilon)(\rho c)_f]/(\rho c)_f$
τ	dimensionless time, tU_o/H

Subscripts

c	cold
eff	effective property
f	fluid
h	hot
s	solid
$\langle\ \rangle$	volume-averaged quantity

concluded that porous cavities do hold a promising potential in regulating skin friction and enhancing the rate of heat transfer. Their results were presented using various dimensionless groups such as the Reynolds number, the Darcy number, the Prandtl number. However, their investigation has merely focused on forced convection aspect of the configuration. In addition, no specific formulation of the effective thermal conductivity of the porous medium was presented. On top of this, the effect of thermal dispersion was not considered in the above work. The mixing of local fluid streams in the presence of a temperature difference across the porous medium yields an increase in the transported energy, which is generally represented by a diffusive heat flux. Subsequently, the inclusion of thermal dispersion effects aids in augmenting the energy transport process and its incorporation in the simulation would, thus, provide a better simulation of the actual problem at hand [9].

The chief objective of the present numerical investigation is to examine the characteristics of a lid-driven flow in a stable thermally-stratified two-dimensional square cavity filled with a water-saturated porous medium. The general formulation of the momentum equation in the presence of a porous medium is employed such that it accounts for the inertial as well as the viscous effects. Thermal dispersion effects have also been incorporated in the mathematical model for all the case studies analyzed in the current investigation. The characteristics of the flow and temperature fields are presented in terms of the Darcy number Da and the Richardson number Ri. The investigation will also explore the significance of the inertial effects and the appropriate measures for depicting the domain where its impact is significant on the heat transfer results. Finally, the investigation was completed by documenting the heat transfer results in the form of an average Nusselt number correlation for the general model over a wide range of Ri. The correlation is essential in demonstrating the enhancement achieved in heat transfer as compared to that given by the conductive mode for the case of a stationary top wall.

2. Analysis

2.1. Mathematical formulation

The configuration described in the present investigation is shown in Fig. 1. The geometry is essentially a two-dimensional square cavity with a side length H. In

addition, the cavity is filled with a porous material that is homogeneous and isotropic. The thermophysical properties of the working fluid and the solid matrix of the porous medium are taken to be constant except for the density variation, which is handled according to the Boussinesq approximation. Furthermore, the solid matrix is made of spherical particles, while the porosity and permeability of the medium are assumed to be uniform throughout the cavity. The choice of a variable-porosity medium is altered in favor of a constant-porosity medium due to the high porosity value considered in this investigation. Moreover, the presence of sharp edges at the corner of the cavity would not make the familiar exponentially decaying porosity model a reasonable choice.

The sliding top wall, which moves from left to right at a constant speed U_0, is maintained at a higher temperature than the stationary bottom wall. Meanwhile, the two vertical walls are subjected to insulated boundary conditions. This produces a configuration with a stable stratification. The local thermal equilibrium condition is invoked here under the presumption of a small temperature difference between the fluid and the solid.

The point governing equations for mass, momentum and energy are transformed to the macroscopic level using the volume-average technique as outlined by Whitaker [10], and later reformulated by Amiri and Vafai [9]. The canonical form of these equations can be expressed as such

$$\nabla \cdot \langle \mathbf{v} \rangle = 0 \tag{1}$$

$$\frac{1}{\varepsilon}\frac{\partial \mathbf{v}}{\partial t} + \frac{1}{\varepsilon^2}\langle(\mathbf{v}\cdot\nabla)\mathbf{v}\rangle = -\frac{1}{\rho_f}\nabla\langle P\rangle^f + \frac{\nu_f}{\varepsilon}\nabla^2\langle\mathbf{v}\rangle - \frac{\nu_f\langle\mathbf{v}\rangle}{K} - \frac{F}{\sqrt{K}}|\langle\mathbf{v}\rangle|\langle\mathbf{v}\rangle - \beta(\langle T\rangle - T_c)\vec{g} \tag{2}$$

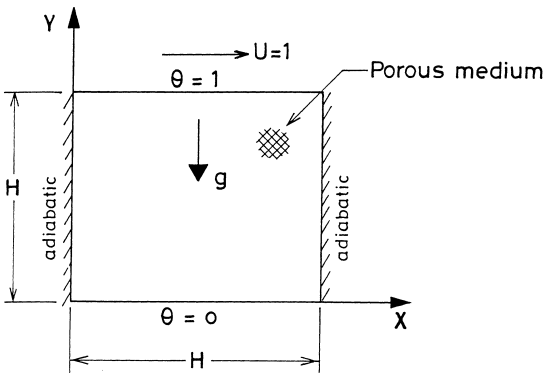

Fig. 1. The configuration of the problem under consideration.

$$\left[\varepsilon(\rho c)_f + (1-\varepsilon)(\rho c)_s\right]\frac{D\langle T\rangle}{Dt} = \nabla\cdot(k_{eff}\cdot\nabla\langle T\rangle) \tag{3}$$

where β is the volumetric expansion coefficient, c_f and c_s the fluid and solid specific heats at constant pressure respectively, $\vec{g}$ the gravitational acceleration vector, k_{eff} is the effective thermal conductivity of the porous medium, ν_f the fluid kinematic viscosity, $\langle P\rangle^f$ the average pressure read off a pressure gage, ρ_f and ρ_s the fluid and solid densities respectively, t stands for time, T for temperature, and $\mathbf{v}$ represents the interstitial velocity vector. It is worth noting that the velocity and the temperature are both taken here as volume-averaged quantities.

Eq. (2), which is referred to here as the generalized form of the momentum equation, allows for a smooth transition between the fluid flow through a porous medium and the Navier–Stokes equation in the space void of a porous medium as $K\to\infty$. The second term on the right-hand side is the Brinkmann term, which accounts for the presence of a solid boundary. The viscous boundary layer in the presence of a porous medium is very thin for most engineering applications [11]. However, its inclusion is essential for the heat transfer calculations. Furthermore, the pressure drop is maintained by the combined effects of the Darcy resistance, represented by the third term, and the inertial effects represented by the quadratic term. The quadratic nature of the inertial effects makes their contribution more noteworthy in hindering the fluid motion as flow activities intensify. In the absence of the inertial effects, Eq. (2) is known as the Brinkmann-extended Darcy model. Further insight into the physical interpretation of the various terms appearing in the above equations are provided in a recent review by Vafai and Amiri [12]. The averaging symbol $\langle\rangle$ will be omitted hereafter for convenience.

The geometric function F and the permeability of a porous medium K are based on Ergun's experimental investigation [13], and is expressed by Vafai [14] as follows

$$F = \frac{1.75}{\sqrt{150\varepsilon^3}} \tag{4}$$

$$K = \frac{\varepsilon^3 d_p^2}{150(1-\varepsilon)^2} \tag{5}$$

where d_p is the solid particle diameter and ε is the porosity of the porous medium. The value of d_p and ε considered for this investigation are 1 mm and 0.9, respectively.

The effective thermal conductivity of a porous medium emerges as a combination of the conductivities of two constituents; a stagnant component and a dispersion component

$$k_{\text{eff}} = k_{\text{e}} + k^{\text{d}} \tag{6}$$

where k_{e} stands for the stagnant conductivity and k^{d} stands for the dispersion conductivity. In the ongoing investigation, the stagnant component is based on the experimental findings of Zehner and Schlüender [15] as follows

$$\frac{k_{\text{e}}}{k_{\text{f}}} = \left(1 - \sqrt{1-\varepsilon}\right) - \frac{2\sqrt{1-\varepsilon}}{1-\lambda B} \times \left[\frac{(1-\lambda)B}{(1-\lambda B)^2}\ln(\lambda B) + \frac{B+1}{2} + \frac{B-1}{1-\lambda B}\right]$$

with

$$\lambda = \frac{k_{\text{f}}}{k_{\text{s}}} \quad \text{and} \quad B = 1.25\left[\frac{1-\varepsilon}{\varepsilon}\right]^{\frac{10}{9}} \tag{7}$$

whereas the dispersion conductivity is determined based on the experimental correlation reported by Wakao and Kaguei [16] given by

$$\frac{k_x^{\text{d}}}{k_{\text{f}}} = 0.5\left[|\mathbf{v}|d_{\text{p}}/\nu_{\text{f}}\right]Pr \tag{8}$$

$$\frac{k_y^{\text{d}}}{k_{\text{f}}} = 0.1\left[|\mathbf{v}|d_{\text{p}}/\nu_{\text{f}}\right]Pr \tag{9}$$

where the modulus of the velocity vector $|\boldsymbol{v}| = \sqrt{u^2+v^2}$ with u and v being the interstitial velocity in x and y directions, respectively.

In accordance with the problem description, the initial and boundary conditions are presented as

$$\mathbf{v} = 0, \quad T = 0 \quad \text{for} \quad t = 0$$

$$\mathbf{v} = (1,0) \quad \text{at} \quad y = H, \quad 0 \le x \le H \quad \text{for} \quad t > 0$$

$$\mathbf{v} = 0 \quad \text{at} \quad y = 0, \quad 0 \le x \le H \quad \text{for} \quad t > 0$$

$$\text{and at} \quad x = 0, H, \quad 0 \le y \le H \quad \text{for} \quad t > 0$$

$$\frac{\partial T}{\partial x} = 0 \quad \text{at} \quad x = 0, H, \quad 0 \le y \le H$$

$$T = T_{\text{c}} \quad \text{at} \quad y = 0, \quad 0 \le x \le H$$

$$T = T_{\text{h}} \quad \text{at} \quad y = H, \quad 0 \le x \le H \tag{10}$$

2.2. Vorticity–stream function formulation

Introducing the formulation of the vorticity Ω and the stream function ψ as

$$u = \frac{\partial \psi}{\partial y}, \qquad v = -\frac{\partial \psi}{\partial x} \tag{11}$$

$$\Omega = \frac{\partial v}{\partial x} - \frac{\partial u}{\partial y} \tag{12}$$

The momentum equation may be accordingly presented in the following form

$$\varepsilon\frac{\partial \Omega}{\partial t} + u\frac{\partial \Omega}{\partial x} + v\frac{\partial \Omega}{\partial y} = \varepsilon\nu_{\text{f}}\left(\frac{\partial^2 \Omega}{\partial x^2} + \frac{\partial^2 \Omega}{\partial y^2}\right) - \frac{\varepsilon^2 \nu_{\text{f}}}{K}\Omega - \frac{F\varepsilon^2}{\sqrt{K}}|\mathbf{v}|\Omega + \frac{F\varepsilon^2}{\sqrt{K}}\left(u\frac{\partial |\mathbf{v}|}{\partial y} - v\frac{\partial |\mathbf{v}|}{\partial x}\right) + \varepsilon^2 g\beta\frac{\partial T}{\partial x} \tag{13}$$

Dimensionless forms of the governing equations will be used to facilitate the handling of the governing equations

$$\varepsilon\frac{\partial \omega}{\partial \tau} + U\frac{\partial \omega}{\partial X} + V\frac{\partial \omega}{\partial Y} = \frac{\varepsilon}{Re}\left(\frac{\partial^2 \omega}{\partial X^2} + \frac{\partial^2 \omega}{\partial Y^2}\right) - \frac{\varepsilon^2}{DaRe}\omega - \frac{F\varepsilon^2}{\sqrt{Da}}|\mathbf{v}|\omega + \frac{F\varepsilon^2}{\sqrt{Da}}\left(U\frac{\partial |\boldsymbol{v}|}{\partial Y} - V\frac{\partial |\boldsymbol{v}|}{\partial X}\right) + \varepsilon^2 Ri\frac{\partial \theta}{\partial X} \tag{14}$$

$$\left(\frac{\partial^2 \Psi}{\partial X^2} + \frac{\partial^2 \Psi}{\partial Y^2}\right) = -\omega \tag{15}$$

$$\sigma\frac{\partial \theta}{\partial \tau} + U\frac{\partial \theta}{\partial X} + V\frac{\partial \theta}{\partial Y} = \left\{\left(\frac{k_{\text{eff},\,x}}{k_{\text{f}}}\frac{\partial^2 \theta}{\partial X^2} + \frac{k_{\text{eff},\,y}}{k_{\text{f}}}\frac{\partial^2 \theta}{\partial Y^2}\right) + \left(\frac{\partial k_{\text{eff},\,x}/k_{\text{f}}}{\partial X}\frac{\partial \theta}{\partial X} + \frac{\partial k_{\text{eff},\,y}/k_{\text{f}}}{\partial Y}\frac{\partial \theta}{\partial Y}\right)\right\}/Pe \tag{16}$$

where the capacity ratio $\sigma = \lfloor\varepsilon(\rho c)_{\text{f}} + (1-\varepsilon)(\rho c)_{\text{s}}\rfloor/(\rho c)_{\text{f}}$, and Pe is the Peclet number. The dimensionless variables appearing in the equations above are defined as such

$$X = \frac{x}{H}, \quad Y = \frac{y}{H}, \quad \tau = \frac{tU_0}{H}, \quad U = \frac{u}{U_0}, \quad V = \frac{v}{U_0}, \quad \omega = \frac{\Omega H}{U_0}, \quad \Psi = \frac{\psi}{HU_0} \quad \text{and} \quad \theta = \frac{T - T_{\text{c}}}{T_{\text{h}} - T_{\text{c}}} \tag{17}$$

The total rate of heat transfer at a given height is

attributed to conductive and convective modes of heat transfer, and can be written in terms of the overall Nusselt number as such

$$\overline{Nu} = -\int_0^1 \left[PeV\theta - \frac{k_{\text{eff},\,y}}{k_{\text{f}}}\frac{\partial\theta}{\partial Y}\right] \mathrm{d}X \tag{18}$$

Unlike the classical flows in the absence of porous media, the incorporation of the effective thermal conductivity in modeling the conductive contribution is a key in providing a more accurate simulation of the energy transport process. This is vivid from the inclusion of the stagnant component, as given by Eq. (7), and the thermal dispersion conductivity in the transverse direction as given by Eq. (9).

The thermophysical properties chosen in this study for the fluid and the solid phase belong to water and copper, respectively. This particular combination of fluid and solid is often associated with porous metal heat exchangers. The numerical data were evaluated at 300 K as such

Copper	Saturated water
$\rho_{\text{s}} = 8933$ kg m^{-3}	$\rho_{\text{f}} = 997$ kg m^{-3}
$c_{\text{s}} = 385$ J kg^{-1} K^{-1}	$c_{\text{f}} = 4179$ J kg^{-1} K^{-1}
$k_{\text{s}} = 400$ W m^{-1} K^{-1}	$k_{\text{f}} = 0.613$ W m^{-1} K^{-1}
	$\mu_{\text{f}} = 855 \times 10^{-6}$ Ns m^{-2}
	$\beta = 0.0033$ K^{-1}

2.3. Numerical scheme, procedure and accuracy considerations

Control-volume approach is employed to handle the governing equations. The momentum and the energy equations may be written in the following format

$$\delta_\phi \frac{\partial\phi}{\partial\tau} + \frac{\partial}{\partial X}\left[U\phi - \Gamma_\phi\frac{\partial\phi}{\partial X}\right] + \frac{\partial}{\partial Y}\left[V\phi - \Gamma_\phi\frac{\partial\phi}{\partial Y}\right] = S_\phi \tag{19}$$

where ϕ stands for either ω or θ with

$$\delta_\phi = \varepsilon,\ \Gamma_\omega = \frac{\varepsilon}{Re},\ S_\omega = \frac{F\varepsilon^2}{\sqrt{Da}}\left(U\frac{\partial|\mathbf{v}|}{\partial Y} - V\frac{\partial|\mathbf{v}|}{\partial X}\right) - \frac{F\varepsilon^2}{\sqrt{Da}}|\mathbf{v}|\omega - \frac{\varepsilon^2}{DaRe}\omega + \varepsilon^2 Ri\frac{\partial\theta}{\partial X} \tag{20a}$$

$$\delta_\theta = 1.0,\ \Gamma_\theta = \frac{1}{Pe},\ S_\theta = \left(\frac{\partial k_{\text{eff},\,x}}{\partial X}\frac{\partial\theta}{\partial X} + \frac{\partial k_{\text{eff},\,y}}{\partial Y}\frac{\partial\theta}{\partial Y}\right)/Pe \tag{20b}$$

The central-differencing format was applied to all the convective and diffusive terms. The transient finite difference equations, Eqs. (14) and (16), were solved using the Alternating Direct Implicit algorithm (ADI). Furthermore, the power-law technique as outlined by Patankar [17] was utilized in conjunction with ADI. The splitting nature offered by the ADI method in each direction facilitates the use of power-law which is solely applicable in a one-dimensional fashion. The convergence of the solution toward a steady state was accelerated by use of the false transient method. Successive over relaxation method (SOR) was employed to solve for the flow kinematics relation represented by Eq. (15). With an improved guess of $\Psi_{i,\,j}^{n+1}$ at hand, $U_{i,\,j}^{n+1}$ and $V_{i,\,j}^{n+1}$ are calculated from the definition of the stream function

$$U_{i,\,j}^{n+1} = \frac{\Psi_{i,\,j+1}^{n+1} - \Psi_{i,\,j-1}^{n+1}}{2\Delta Y} \quad \text{and} \quad V_{i,\,j}^{n+1} = \frac{\Psi_{i-1,\,j}^{n+1} - \Psi_{i+1,\,j}^{n+1}}{2\Delta X} \tag{21}$$

The vorticity on the boundaries is expressed in terms of the primitive velocity variables as

$$\omega_{i,\,1} = \frac{\left(-4U_{i,\,2} + U_{i,\,3}\right)}{2\Delta Y},\qquad \omega_{i,\,N} = \frac{\left(-3U_o + 4U_{i,\,N-1} - U_{i,\,N-2}\right)}{2\Delta Y},$$

$$\omega_{1,\,j} = \frac{\left(4V_{2,\,j} - V_{3,\,j}\right)}{2\Delta X} \quad \text{and} \quad \omega_{M,\,j} = \frac{\left(-4V_{M-1,\,j} + V_{M-2,\,j}\right)}{2\Delta X} \tag{22}$$

Steady state condition was recognized when the difference in the maximum norm of both the vorticity and the temperature values became less than 10^{-6}.

A couple of measures were introduced to assess the validity of the numerical scheme. First, the sensitivity of the numerical outcome was examined by systematically increasing the mesh size until further refinement of the mesh size agreed to better than one percent difference in the computational solution. A mesh size of 81×81 was found adequate to simulate the flow and thermal responses of the problem under consideration. Fig. 2 depicts the distribution of the horizontal velocity and the temperature distribution inside the cavity at $X = 0.5$ being plotted against the vertical coordinate for $Da = 0.1$, $Gr = 10^4$ and $Ri = 1.0$. As can be seen from Fig. 2, the results confirm the choice of the mesh size. The second measure for the validation process composed of comparing the outcome of the numerical code against a reliable documented

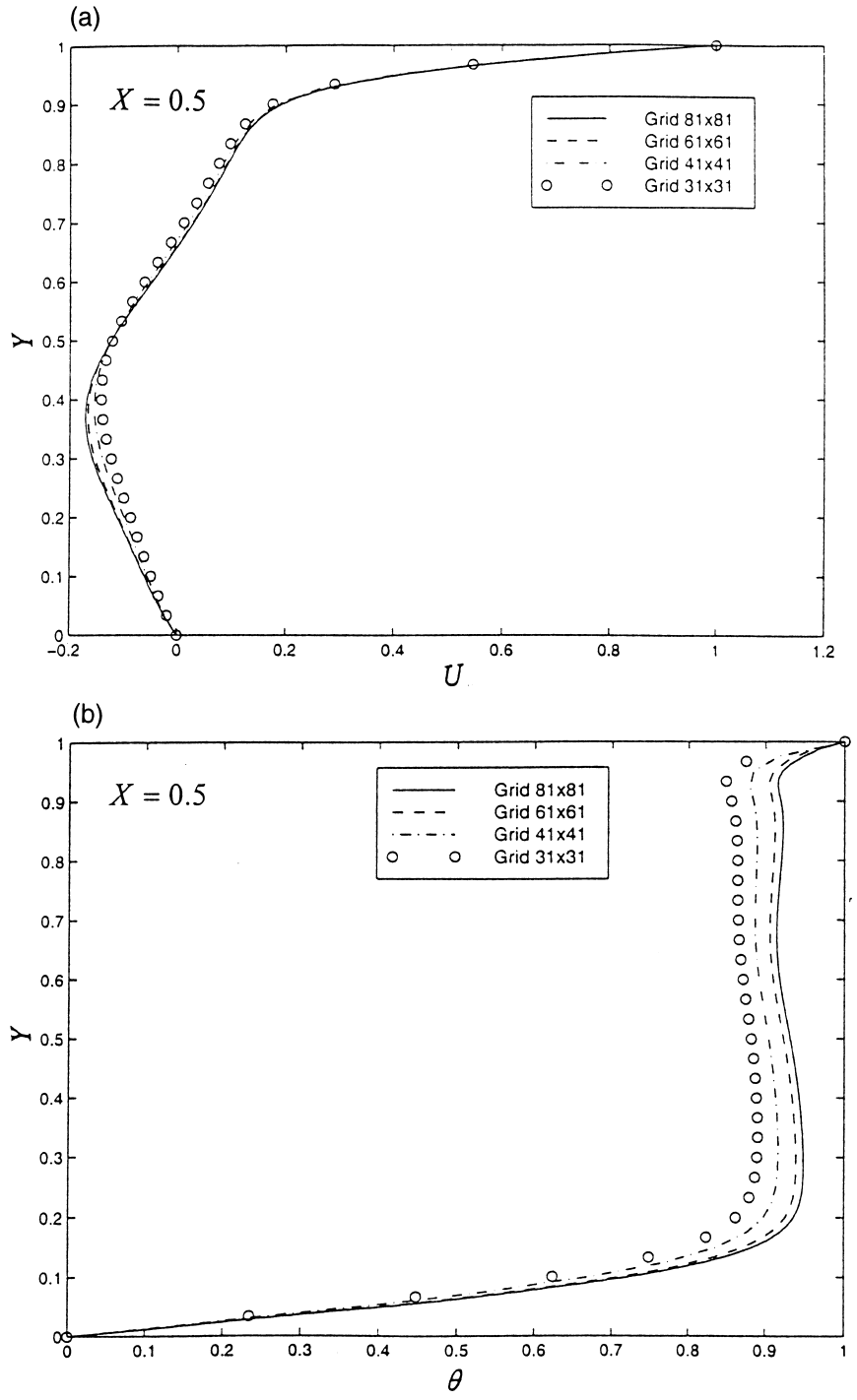

Fig. 2. Grid independence evaluation for $Da = 0.1$ and $Ri = 1.0$.

Table 1
Comparison of the maximum and minimum values of the velocity components at the mid-section of the cavity between the present work and those of Iwatsu et al. [5]

	$Ri = 1 \times 10^{-2}$		$Ri = 6.25x10^{-4}$	
	Present	Iwatsu et al. [5]	Present	Iwatsu et al. [5]
U_{min}	−0.2122	−0.2037	−0.3099	−0.3197
U_{max}	1.000	1.000	1.000	1.000
V_{min}	−0.2506	−0.2448	−0.4363	−0.4459
V_{max}	0.1765	0.1699	0.2866	0.2955

work. Also, a finite-element software package (FIDAP) was used to execute the same validation cases for an additional source of confidence. The numerical study reported by Iwatsu et al. [5] was chosen as a basis for this comparison. Since their results were merely generated for a lid-driven cavity in the absence of a porous medium with air being the working fluid; the code was executed for a highly permeable medium ($Da = \infty$). The outcome of the comparison, which was conducted for $Gr = 10^2$, is summarized in Tables 1 and 2. It reveals that the maximum discrepancy between the present numerical results and that of Iwatsu et al. [5] is equal or less than 4% for the velocity and Nusselt number predictions. What is more, the results in Table 2 show that the FIDAP predictions, which is presented for the Nusselt number predictions for brevity, are in better overall agreement with the present numerical investigation with a difference of 3% or less. Accordingly, the comparisons reveal a satisfactory agreement and would, hence, boost confidence in the generated results.

3. Results and discussions

The effects of the Darcy number and the Richardson number on the flow and thermal behaviors of the porous cavity are investigated. The Darcy number, which is directly proportional to the permeability of the porous medium, was set to vary between 0.001–0.1. The Richardson number is defined as the ratio of Gr/Re^2, which reflects a dominant conduction mode when $Gr/Re^2 \geq O(1)$, while it resembles similar lid-driven cavity flow behavior for a non-stratified fluid when $Gr/Re^2 \leq O(1)$ [5]. The Richardson number in the ongoing investigation was varied in the range of 10^{-4}–5.0 by varying the Reynolds number while the Grashof number was fixed at 10^4. As mentioned earlier, the investigation is primarily concerned with the impact of the inertial effects on the flow and heat transfer inside the porous cavity. Hence, comparisons are made between the generalized model and the Brinkmann–extended Darcy model (hereafter B–e Darcy model). What is more, these comparisons are demonstrated by plotting the predicted velocity and temperature fields at halfway through the horizontal distance against the vertical coordinate. However, the velocity field has been displayed using the horizontal velocity component only for brevity. In addition, contour plots for the stream function as well for the temperature inside the cavity are documented.

Table 2
Comparison of the average Nusselt number at the top wall between the present solution and that of Iwatsu et al. [5]

Parameter	Present	Iwatsu et al. [5]	FIDAP
$Ri = 1 \times 10^{-2}$	2.01	1.94	1.99
$Ri = 6.25 \times 10^{-4}$	3.91	3.84	4.02
$Ri = 1 \times 10^{-4}$	6.33	6.33	6.47

3.1. Effect of the Darcy number

Fig. 3 depicts the horizontal velocity and the temperature distributions for a fixed value of $Ri = 10^{-2}$. The results show an increase in the velocity and temperature magnitudes predicted by the B–e Darcy model due to omission of inertial effects. Moreover, this increase is more pronounced for higher values of the Darcy number due to increase in flow conductance, i.e., the permeability of the porous structure. Apparently, the increase in the Darcy number induces flow activity deeper into the cavity, which causes more energy to be carried away from the sliding top wall toward the bottom. As a result, higher temperature readings are predicted when descending farther inside the cavity. This confines the conduction regime to a narrow region from the bottom wall. In the conduction dominated region, the temperature predicted by the B–e Darcy model remains slightly higher than that predicted by the generalized model. This is most likely due to some lingering flow activities in this particular region. Overall, the decrease in the Darcy number contributes further to flow suppression sustained by the stable stratification.

Fig. 4 displays the results for $Ri = 6.25 \times 10^{-4}$ and confirms the above stated observations and, also, indicates that the inertial effects hinder momentum and energy transport. However, the impact of the inertial effects on thermal behavior seems to be of less significance though, except for $Da = 0.1$ where considerable elevation in the flow and thermal activities is manifested. It is noted that the temperature profile predicted by the B–e Darcy model for $Da = 0.1$ dips slightly toward the center of the cavity. This is due to the presence of a relatively active fluid motion that

approaches zero in the central region. Owing to the larger magnitude of velocity predicted by the B–e Darcy model; its impact on thermal behavior is obviously more pronounced.

In order to assess global influence of the inertial effects, the streamlines and isotherms distribution inside the entire cavity is presented for $Ri = 6.25 \times 10^{-4}$ in Figs. 5 and 6 using the generalized model and the B–e Darcy model, respectively. As seen from Fig. 5, the streamlines collapse together toward the right top corner where the sliding top wall impinges on the vertical right wall. In addition, the

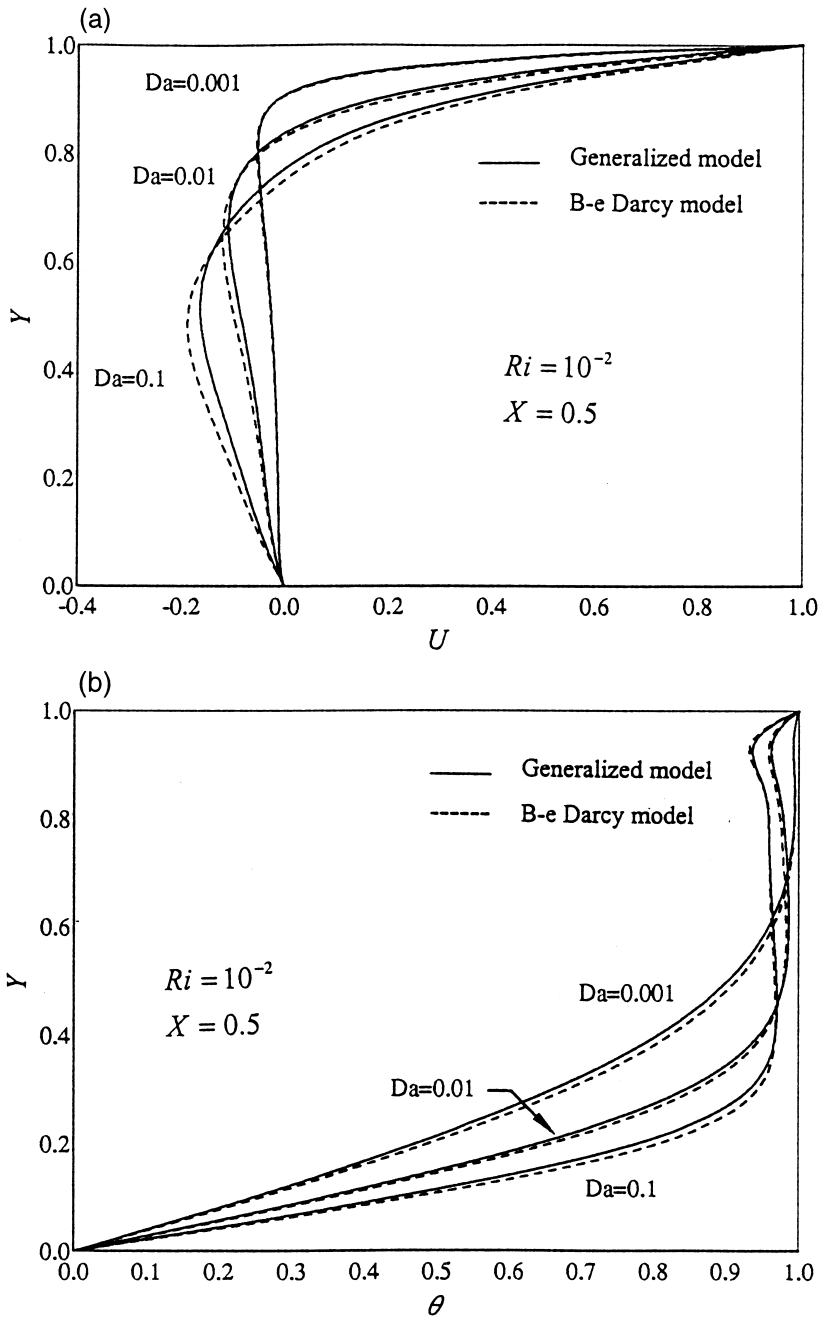

Fig. 3. The horizontal velocity and the temperature fields presented at different values of the Darcy number.

results show that the increase in *Da* value causes the center of the vortex to move downward toward the center of the cavity. On the other hand, the decrease in *Da* precludes the streamline intensity level and prevents downward flow penetration, which causes the streamlines to stretch too thin in a shallow depth away from the top wall. Meanwhile, the isotherms appear to assume the sliding top wall temperature in the bulk of the cavity especially toward the right vertical wall, which implies that the fluid is well mixed due to the mechanically-induced convection. It is apparent that the increase in *Da* expands the domain for which the

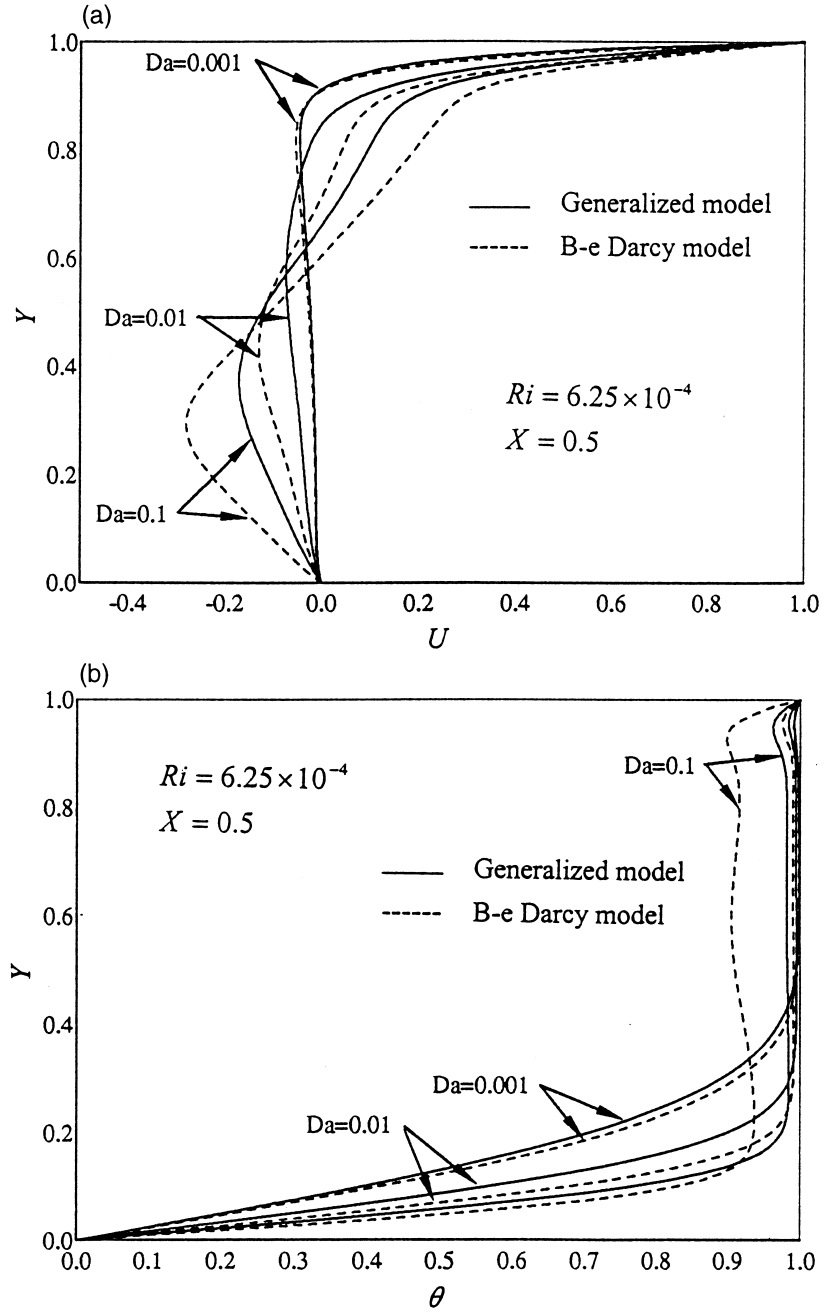

Fig. 4. The horizontal velocity and the temperature fields presented at different values of the Darcy number.

convection regime is dominant. Consequently, the temperature gradients in the vertical direction become steeper toward the bottom wall where the conduction regime is dominant due to minimal flow activities. These effects are more pronounced for the predictions given by the B–e Darcy model as depicted in Fig. 6. The center of the vortex has been further pulled toward the top right corner as *Da* increases. Moreover, the region underneath the sliding top wall is observed to grow relatively thickness wise since the inertial effects are silenced. The increase in flow predictions by the B–e Darcy model has relatively caused further energy to be carried away from the top wall and into the cavity.

The presentation of the field variables is further stretched to depict the case for which the buoyancy effects are of equal weight to the sliding lid, i.e., $Ri = 1.0$. The contour results, which are generated using the generalized model, are shown in Fig. 7. Moreover, the contour intensity labeling was altered due to the clustering of the lines near the sliding lid for the streamlines and toward the bottom wall for the isotherms. Instead, the maximum and the minimum values were displayed on each graph. The results show weakened

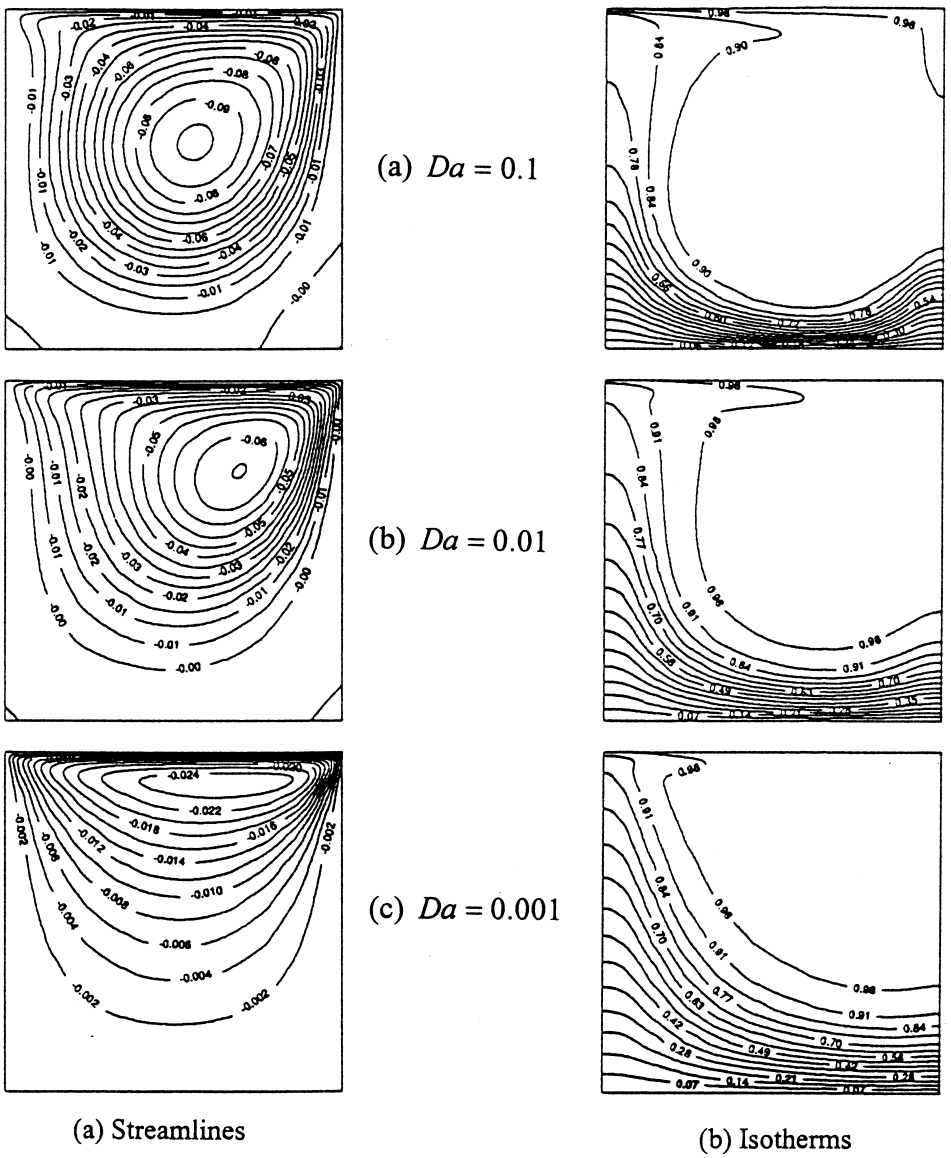

Fig. 5. The streamline and the isotherm patterns illustrated for $Ri = 6.25 \times 10^{-4}$ using the generalized model.

flow activities due to stratification, which is suggested by the formation of a separate cell in the lower half of the cavity. This formed cell appears to grow in size for $Da = 0.01$ and ultimately separates into minor cells as the Darcy number decreases to $Da = 0.001$. Apparently, much smaller contour levels seems necessary to capture these minor cells toward the bottom corners of the cavity, which should cause further clustering of the lines. The readings from the temperature contours point out that conduction is the dominant mode of heat transfer and that convection heat transfer is confined to the upper right corner. As noted earlier, this confined zone enlarges somewhat as the openness in the porous medium increases which allows more fluid penetration into the porous medium.

3.2. Effect of the Richardson number

Fig. 8 illustrates the velocity and the temperature fields for $Ri = 10^{-2}$, 2.5×10^{-3} and 1.11×10^{-3} with a fixed value of Darcy number that is equal to 0.1. As displayed in the figure, the flow activity inside the cavity intensifies as the Richardson number decreases. Apparently, the discrepancy in the magnitude of the

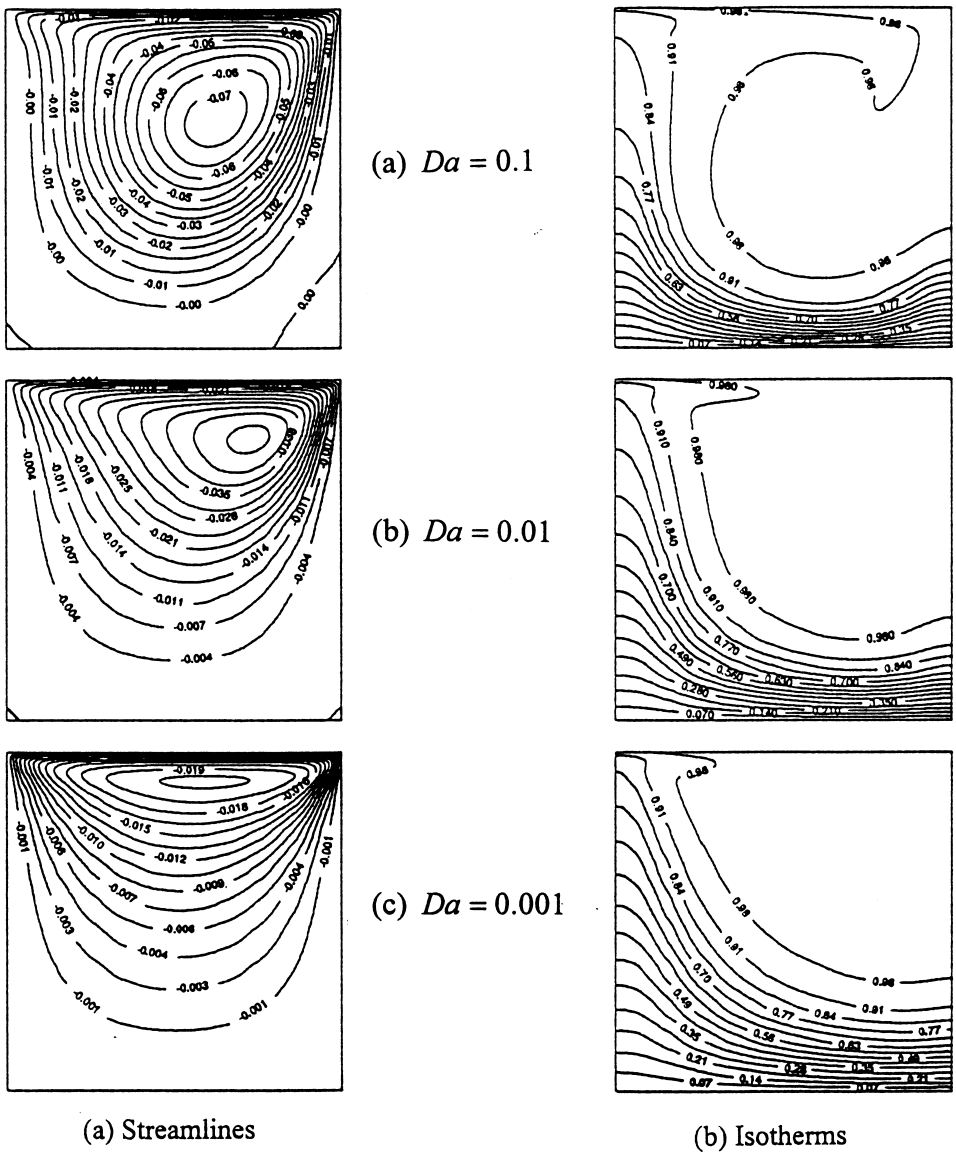

Fig. 6. The streamline and the isotherm patterns illustrated for $Ri = 6.25 \times 10^{-4}$ using the B–e Darcy model.

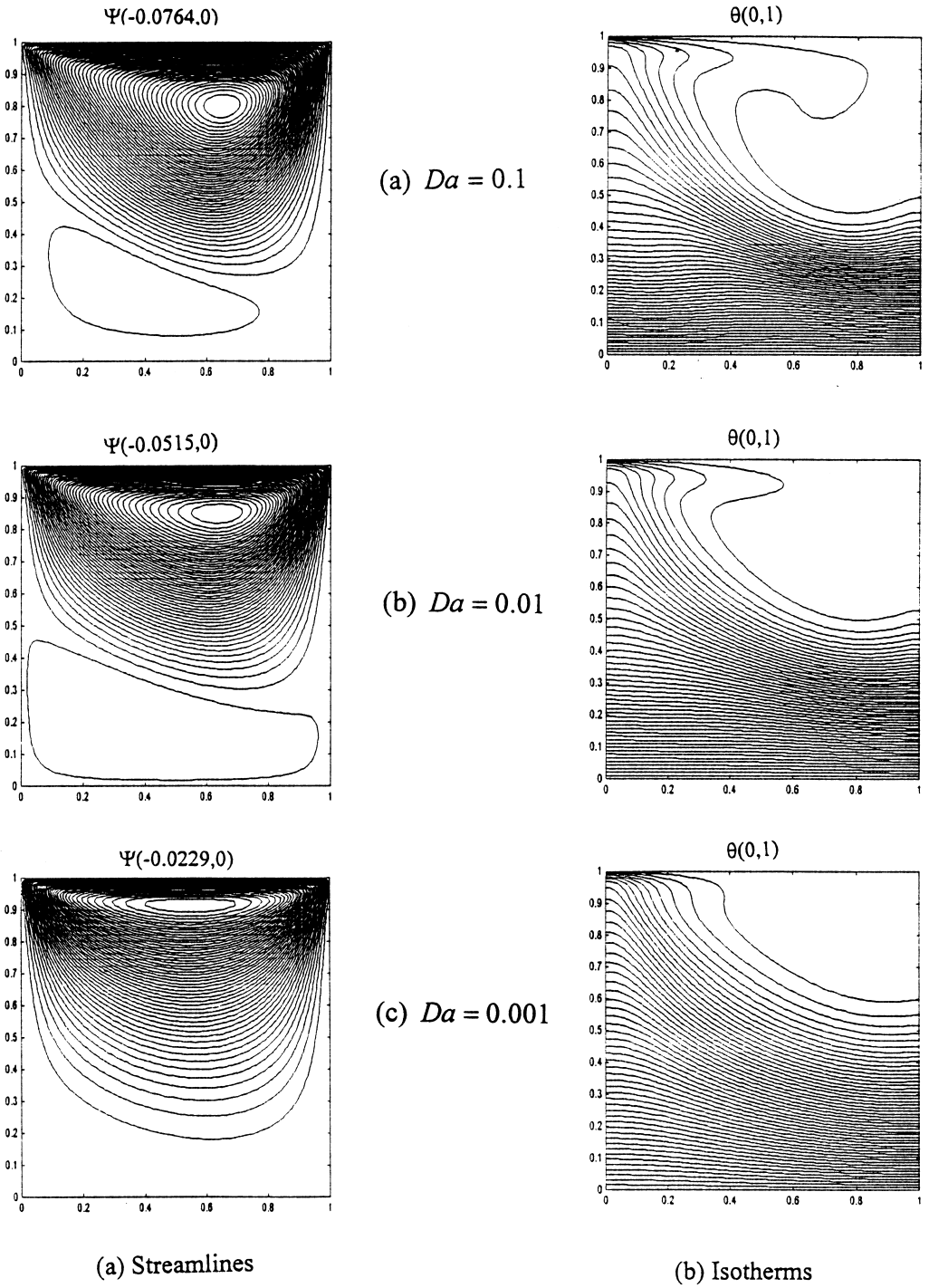

Fig. 7. The streamline and the isotherm patterns illustrated for $Ri = 1.0$ using the generalized model.

velocity predicted by the two models is directly proportional to the increase in the mechanical effect offered by the sliding wall. The discrepancy in velocity predictions between the two models has subsequently impacted the temperature results. However, the deviation in temperature profile between the generalized model and the B–e Darcy model seems to be less pronounced for this particular Darcy number. Apparently,

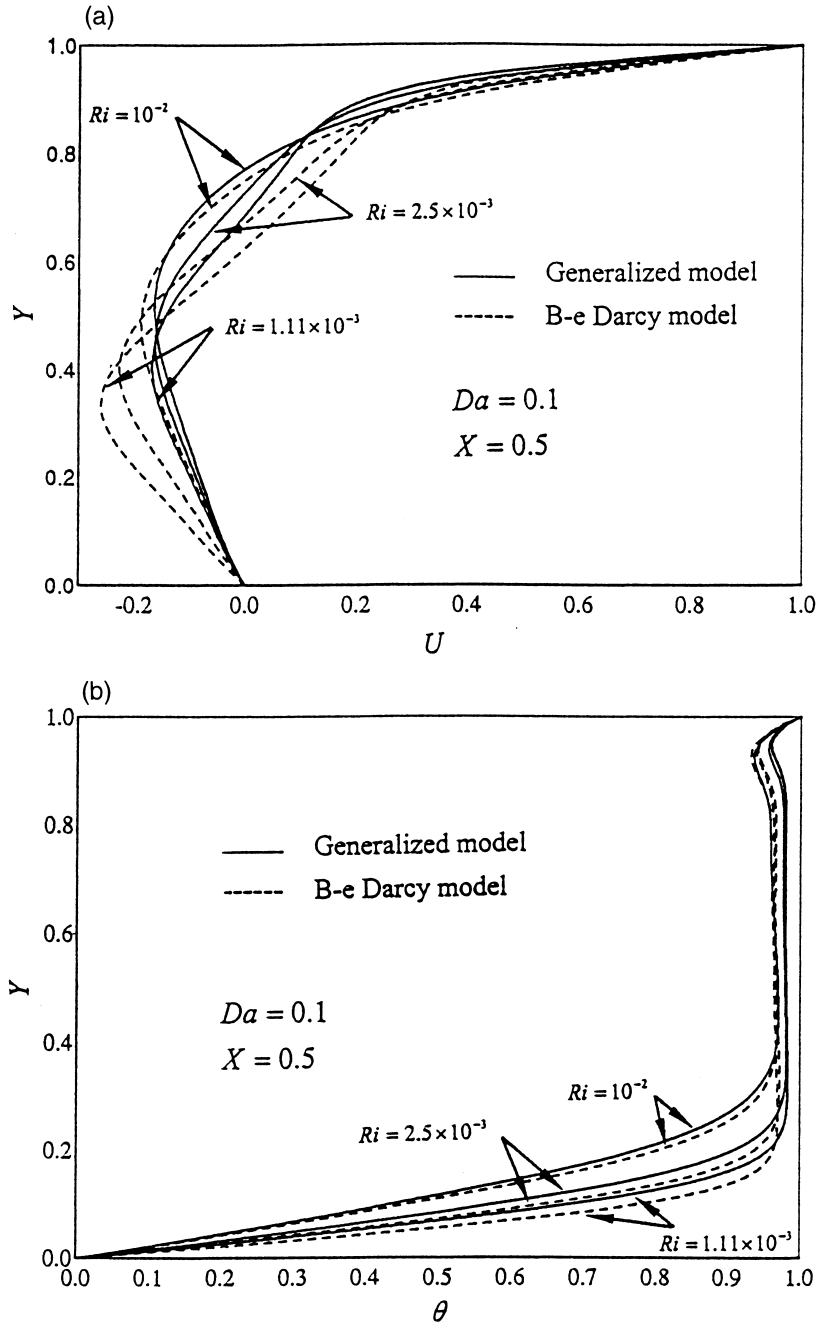

Fig. 8. The horizontal velocity and the temperature fields presented at different values of the Richardson number.

further increase in the Ri value will inhibit fluid motion due to the strong stratification in the fluid layers.

3.3. Nusselt number correlation

Due to the extensive number of cases being performed in the ongoing investigation, the overall Nusselt number predictions for the generalized model in the range of $0.001 \leq Da \leq 0.1$ and $10^{-4} \leq Ri \leq 5.0$ were documented in the form of the following correlation:

$$\overline{Nu} = 0.119(Re)^{0.78}(Ri)^{0.29}\left[0.39 + 5.3 \times 10^{-3} ReDa^{0.57}\right]$$

The correlation was found to fit the numerical predictions with a maximum discrepancy of 17% occurring at $Da = 0.1$ and $Ri = 0.1$. A sample of the relative discrepancies between the correlation and the actual numerical predictions are listed in Table 3 for a handful of Ri values at $Da = 0.1$. The results in Table 3 clearly reflect the implications of thermal stratification in hindering fluid motion and, thus, the heat transfer level. The correlation suggests that heat transfer rate is strongly dependent on Re as compared to Da and Ri. Moreover, the small coefficient of the $ReDa$ term was deliberately retained to highlight the significant increase in Nusselt number predictions due to the presence of a porous medium. It is obvious here that the increase in the Da value will bring about an increase in the Nusselt number since more fluid can penetrate into the porous matrix. Several additional features could also be explored upon further stretching the openness of the porous structure toward classical cavity flows ($Da = \infty$), which invites further investigation in this area.

4. Conclusions

The problem of a laminar lid-driven square cavity filled with a water-saturated porous medium has been investigated. The characteristics of the flow and temperature fields in the porous cavity were analyzed under stable thermal stratification with emphasis on the influence of the quadratic inertial effects. In addition, pertinent dimensionless groups such as the Darcy number and the Richardson number were utilized in the undergoing analysis. The results imply that the inertial effects retard momentum and energy transport. However, such effects are found to be more pronounced for the flow behavior, which makes the outcome of the B–e Darcy model to overpredict the results produced by the generalized model especially at higher values of Da or lower values of Ri. Furthermore, the increase in Da was found to induce flow activities causing an increase in the fraction of energy transport by means of convection. This conclusion is also valid for a decrease in Ri.

The overall observation indicates that a stable stratification suppresses flow motion, which is further strengthened by the presence of a porous medium in the cavity. Finally, the numerical results for the generalized model were documented by developing a correlation based on the predicted average Nusselt number in the range of $Da = 0.001$–0.1 and $Ri = 10^{-4}$–5.0.

Table 3
A sample of the overall Nusselt number discrepancies between the correlation and the actual numerical predictions presented for $Da = 0.1$

Ri	$\overline{Nu}$ (numerical)	$\overline{Nu}$ (correlation)	Percentage difference
0.01	12.56	12.46	0.6
0.1	3.92	4.59	17.1
1.0	2.31	2.31	0.0
2.5	2.14	1.91	10.7
5.0	1.83	1.68	8.2

Acknowledgements

This work was supported by the Scientific Research Council under Grant number 99/11-7-35.

References

[1] U. Ghia, K.N. Ghia, C.T. Shin, High Re solution for incompressible flow using Navier–Stokes equations and a multigrid method, J. Comput. Phys 48 (1982) 387–411.
[2] M. Morzynski, C.O. Popiel, Laminar heat transfer in a two-dimensional cavity covered by a moving wall, Numerical Heat Transfer 13 (1988) 265–273.
[3] R. Schreiber, H.B. Keller, Driven cavity flows by efficient numerical techniques, J. Comput. Phys 49 (1983) 310–333.
[4] A.A. Mohamed, R. Viskanta, Combined surface shear stress and buoyancy-driven convection in a shallow cavity, in: Proceedings of the AIAA/ASME Thermophysics and Heat Transfer Conference, 1990.
[5] R. Iwatsu, J.M. Hyun, K. Kuwahara, Mixed convection in a driven cavity with a stable vertical temperature gradient, Int. J. Heat Mass Transfer 36 (1993) 1601–1608.
[6] J.R. Koseff, R.L. Street, The lid-driven cavity flow: a synthesis of quantitative and qualitative observations, ASME J. Fluids Engng 106 (1984) 390–398.
[7] A.K. Prasad, J.R. Koseff, Combined forced and natural convection heat transfer in a deep lid-driven cavity flow, Int. J. Heat Fluid Flow 17 (1996) 460–467.

[8] K. Vafai, P.C. Huang, Analysis of heat transfer regulation and modification employing intermittently emplaced porous cavities, ASME J. Heat Transfer 116 (1994) 155–164.
[9] A. Amiri, K. Vafai, Analysis of dispersion effect and non-thermal equilibrium, non-Darcian variable porosity incompressible flow through porous media, Int. J. Heat Mass Transfer 37 (1994) 939–954.
[10] S. Whitaker, Simultaneous heat, mass, and momentum transfer in porous media: a theory of drying, Advances in Heat transfer 13 (1977) 119–203.
[11] K. Vafai, C.L. Tien, Boundary and inertia effects on flow and heat transfer in porous media, Int. J. Heat Mass Transfer 108 (1981) 195–203.
[12] K. Vafai, A. Amiri, Non-Darcian effects in confined forced convective flows, in: D. Ingham, I. Pop (Eds.), Transport Phenomena in Porous Media, Pergamon, UK, 1998, pp. 313–329.
[13] S. Ergun, Fluid flow through packed columns, Chem. Engng. Pro 48 (1952) 89–94.
[14] K. Vafai, Convective flow and heat transfer in variable porosity media, J. Fluid Mech 147 (1984) 233–259.
[15] P. Zehner, E.U. Schlünder, Thermal conductivity of granular materials of moderate temperatures, Chem. Ingr. Tech 42 (1970) 941–993.
[16] N. Wakao, S. Kaguei, Heat and Mass Transfer in Packed Bed, 1st ed., Gordon and Breach, New York, 1980.
[17] S.V. Patankar, Numerical Heat Transfer and Fluid Flow, 1st ed., Hemisphere, New York, 1980.